Hydrogen accommodation in Zr second phase particles: Implications for H pick-up and hydriding of Zircaloy-2 and Zircaloy-4.

P.A. Burr[a,b], S.T. Murphy[a], S.C. Lumley[a,c], M.R. Wenman[a,*], R.W. Grimes[a]

[a] *Centre for Nuclear Engineering and Department of Materials, Imperial College London, London, SW7 2AZ, UK.*
[b] *Institute of Materials Engineering, Australian Nuclear Science & Technology Organisation, Menai, New South Wales 2234, Australia.*
[c] *Nuclear Department, Defence Academy, HMS Sultan, Gosport, Hampshire, PO12 3BY, UK.*

Abstract

Ab-initio computer simulations have been used to predict the energies associated with the accommodation of H atoms at interstitial sites in α, β-Zr and Zr-M intermetallics formed with common alloying additions (M = Cr, Fe, Ni). Intermetallics that relate to the Zr_2(Ni,Fe) second phase particles (SPPs) found in Zircaloy-2 exhibit favourable solution enthalpies for H. The intermetallic phases that relate to the Zr(Cr,Fe)$_2$ SPPs, found predominantly in Zircaloy-4, do not offer favourable sites for interstitial H. It is proposed that Zr(Cr,Fe)$_2$ particles may act as bridges for the migration of H through the oxide layer, whilst the Zr_2(Ni,Fe)-type particles will trap the migrating H until these are dissolved or fully oxidised.

Keywords: A. Zirconium, A. Intermetallics, C. Hydrogen absorption

1. Introduction

For the past five decades, Sn-containing Zr alloys, such as Zircaloys, have been widely used for nuclear fuel cladding and internal components of light water nuclear reactors[1]. To improve their corrosion resistance, Zircaloy-2 (or

*Corresponding author. Tel: +44 (0)2075946763
E-mail address: m.wenman@imperial.ac.uk

Zry-2) also contain small amounts of Fe, Cr and Ni, which precipitate out as SPPs due to their low solid solubility in α-Zr.

Later alloy development led to the formulation of Zry-4, an alloy with much lower Ni content. The reduction of Ni content in Zry-4 resulted in a reduced H pick-up fraction (HPUF) of the alloy without compromising the oxidation resistance[1]. However, the mechanism through which the HPUF is affected by the presence of Ni is still not well understood. There is, nevertheless, general agreement that SPP composition, size and morphology play a key role[3].

There are many theories as to how intermetallics influence corrosion and H pickup but all are subject to challenge[4–8]. Hatano *et al.*[4] suggested that as the oxide layer thickens, the larger SPPs residing at the oxide-metal interface will oxidise more slowly than the surrounding Zr. These partially metallic particles could then act as a H migration pathway (bridge) through the oxide layer. It has been noted by Shaltiel *et al.*[9] that Laves-phase SPPs of the $Zr(Fe,Cr)_2$ type have a tendency to absorb H. Furthermore, the ratio of Fe to Cr seems to influence H absorption. As SPPs are irradiated the Fe dissolves out first, therefore the ratio of Fe-Cr will change and concomitantly the capacity for H absorption. This may lead to a release of H into the α-Zr matrix phase late in fuel life, which could accelerate hydriding of the cladding. Equally, subsequent annealing of SPPs, heated up during the early stage of dry storage of fuel, could reabsorb H from the matrix into recrystallized SPPs and hence be beneficial in reducing available H for hydride reorientation. At present there is little data regarding which traps for H are most efficient.

In this paper we employed density functional theory (DFT) to calculate the solution enthalpies of H in the various binary intermetallic SPPs and compares these to the solution enthalpies of H in both α and β-Zr phases. The two most common SPPs are the ternary $Zr(Cr,Fe)_2$ (especially in Zry-4) and $Zr_2(Fe,Ni)$ (in Zry-2). Whilst it has been reported that binary phases do not tend to form in Zr alloys [10–12], an investigation of the simple binary systems is important, in the first instance, to understand the role that individual alloying elements play in the interaction between H and the intermetallic phases. Consequently,

this allows us to determine which SPPs are likely to behave as described by Hatano's model, if at all.

Cr forms three intermetallic phases with Zr: the cubic α phase and the hexagonal β and γ phases. All three have the same stoichiometric formula $ZrCr_2$ and are all Laves phases, termed *C15*, *C36* and *C14* respectively (see Table 1 for further details). Even though the stable phase at reactor operating temperature is α-$ZrCr_2$, there have been many reports of both cubic[13–17] and hexagonal[10–12, 15–20] structures in Zr alloys, therefore all three have been considered here. Although the Zr-Ni binary system includes numerous intermetallic phases[21], Zr-Ni SPPs tend to be stable as Zr rich phases, in particular tetragonal Zr_2Ni. Fe is found in the $ZrCr_2$-type SPPs as well as in the Zr_2Ni-type, therefore the *C15*, *C36* and *C14* $ZrFe_2$ Laves phase and the Zr_2Fe phase have all been studied. Figure 1 contains schematic representation of unit cells of each of the intermetallic phases described above.

2. Computational Methodology

All DFT simulations were carried out using CASTEP 5.5[22]. Ultra-soft pseudo potentials with a consistent cut-off energy of 450 eV were used throughout. Previous work by Domain *et al.*[23] demonstrated that the Generalized Gradient Approximation (GGA) is better suited than the Local Density Approximation to describe the exchange-correlation functional of solid Zr. Therefore, the Perdew Burke and Ernzerhof (PBE)[24] parametrisation of the GGA was adopted for this study. A high density of **k**-points was employed for the integration of the Brillouin Zone, following the Monkhost-Pack sampling scheme[25]: the distance between sampling points was maintained as close as possible to $0.030\,\text{Å}^{-1}$ and never above $0.035\,\text{Å}^{-1}$. The fast fourier transform grid was set to be twice as dense as that of the wavefunctions, with a finer grid for augmentation charges scaled by 2.3. Due to the metallic nature of the system, density mixing and Methfessel-Paxton[26] cold smearing of bands were employed with a width of 0.1 eV. Testing was carried out to ensure a convergence of 10^{-3} eV/atom was

achieved with respect to all of the above parameters. All calculations were spin polarised and no symmetry operations were enforced.

The energy convergence criterion for self-consistent calculations was set to 1×10^{-6} eV. Similarly robust criteria were imposed for ionic energy minimisation: energy difference $< 1 \times 10^{-5}$ eV, forces on individual atoms $< 0.01\,\text{eV}\,\text{Å}^{-1}$ and stress component on cell < 0.05 GPa (for constant pressure simulations).

All non-defective structures were relaxed at constant pressure (both the crystal's lattice parameters and ion positions within the supercells were subject to energy minimisation). Relaxed structures were then employed for simulations containing H interstitial defects. Defect simulations were performed both at constant volume (cell parameters constrained to preserve the perfect supercell's shape and volume) and at constant pressure; these replicate dilute and alloying conditions respectively.

3. Results and Discussion

3.1. α and β-Zr

When considering the effective H concentration it is important to bear in mind that the solubility of H in α-Zr is 50–60 *wt* ppm at the operating temperature of a pressurised water reactor of 300 °C[27, 28]. For α-Zr, calculations with a simple H interstitial defect were performed for supercells containing up to 150 atoms ($5 \times 5 \times 3$); yielding an effective defect concentration of 73.7 *wt* ppm H, therefore only slightly above the reported solubility limit. For β-Zr the solubility limit of H is orders of magnitude larger[27].

The lattice parameters and enthalpy of formation of each phase investigated were presented in previous work[29] and are in agreement with values available in the literature. In addition, the dissociation energy and dimer length of the H_2 molecule were calculated to be 4.53 eV and 752 pm respectively, in excellent agreement with experimental values, 4.48 eV and 746 pm[30].

α-Zr presents five sites for interstitial occupancy: a tetrahedral site in Wyckoff position[31] $4f$ (with $z = \frac{5}{8}$), an octahedral site ($2a$), an hexahedral site ($2d$),

a basal trigonal site ($2b$), and a non-basal trigonal site ($12k$, with $x = \frac{4}{9}$, $z = \frac{5}{12}$) — the latter three were found to be metastable for H occupancy (i.e. upon energy minimization the H atom relaxes into either the tetrahedral or octahedral sites). β-Zr has stable tetrahedral $12d$ and octahedral $6b$ interstitial sites. A trigonal interstitial site also exists ($24h$, with $y = \frac{1}{3}$), however, this too was found to be unstable for H occupancy.

The enthalpy of solution of an isolated H atom in bulk metal, E_{H}^{sol}, according to reaction 1, was calculated using equation 2,

$$\mathrm{M_{x(s)}} + \tfrac{1}{2}\mathrm{H_{2(g)}} \rightarrow \mathrm{M_xH_{(s)}} \tag{1}$$

$$E_{\mathrm{H}}^{sol} = E^{\mathrm{DFT}}_{\mathrm{M_xH_{(s)}}} - E^{\mathrm{DFT}}_{\mathrm{M_{x(s)}}} - \tfrac{1}{2}E^{\mathrm{DFT}}_{\mathrm{H_{2(g)}}} \tag{2}$$

where M is a metal simulated with a supercell containing x atoms.

The calculated values of solution enthalpies for interstitial H in pure Zr are presented in Table 2, together with reference values from both experimental and other *ab-initio* simulations.

In α-Zr, it was found that H exhibits a slight preference of the tetrahedral site over the octahedral site by $-0.086\,\mathrm{eV}$, however, given the small energy difference between the two sites, H interstitial atom will probably occupy both sites at reactor temperatures. Previous studies by Domain *et al.*[23] record a similar relative preference for the tetrahedral site over the octahedral site, with a similar energy difference, however, their values were lower by $0.13\,\mathrm{eV}$. This discrepancy is mostly accounted for by the calculation of the H_2 molecule: the dissociation energy calculated by Domain *et al.*[23] was $0.26\,\mathrm{eV}$ smaller per hydrogen dimer.

In β-Zr, a the same preference for tetrahedral site was observed, but by a larger margin: $-0.21\,\mathrm{eV}$. Because octahedral sites in β-Zr are anisotropic (slightly compressed in one dimension), the periodic repetition of such defects causes the structure to deform tetragonally. In order to remove this computational artefact, these simulations were carried out with constraints on the cell such that a change in volume was allowed but without any change in cell shape ($a = b = c$ and $\alpha = \beta = \gamma = 90°$ at all times).

3.2. Intermetallics of Zr

When comparing defect energies across different phases, ideally the supercells of all solids investigated should have the same number of atoms to ensure that the defect concentrations are identical. However, differences in crystal structures means that this is not possible. In order to minimise interactions between the defects and their replicas, large supercells were adopted, emulating a dilute H concentration in the materials, and all supercells were chosen to be as regular as possible (i.e. the total lengths of the supercells in the $\boldsymbol{x}$, $\boldsymbol{y}$ and $\boldsymbol{z}$ directions are roughly equal, see Table 1).

Starting from the relaxed structure of a perfect intermetallic phase, a series of simulations were carried out, each with an H atom placed at one of the possible interstitial symmetry sites. This was repeated for every intermetallic phase; in each case the lowest energy site is reported in Table 3. It was found that the lowest energy sites, across all intermetallic phases, were always tetrahedral; and particularly favourable were the ones with a larger Zr/M ratio of neighbouring atoms. The difference in solution enthalpy for H between a constant pressure and a constant volume simulation for a given H defect was consistently below 10^{-2} eV, therefore the latter are omitted from Table 3. Finally, the table contains a comparison of solution enthalpies of H in the various intermetallics relative to α-Zr. A comparison with β-Zr was considered less useful as an earlier study[29] showed that the intermetallics are soluble in the β phase.

The $ZrCr_2$ and $ZrFe_2$ Laves phases that relate to the most common SPP found in Zry-4, offer unfavourable sites for H interstitial defects, compared to α and β-Zr. In fact, the enthalpy of solution in $ZrFe_2$ is actually positive. Since none of the Laves phase intermetallics for either Cr or Fe retain H compared to α-Zr, it seems unlikely $Zr(Cr,Fe)_2$ will offer any more favourable sites. This finding is consistent with the H-uptake model of Hatano *et al.*[4], in that this type of SPP may act as a bridge for H diffusion through the oxide layer, provided it retains a partially metallic form in the surrounding ZrO_2, as suggested by Lelièvre *et al.*[8]. Conversely, Zr_2Fe and Zr_2Ni, which relate to the Zr-rich SPPs found in Zry-2, provide sites with low H solution enthalpy: Zr_2Fe similar to

α-Zr but Zr_2Ni significantly lower than either α or β-Zr. Thus, if the solid solution Zr_2(Fe,Ni) was to behaves similarly to its binary end members Zr_2Fe or Zr_2Ni, these SPPs would preferentially retain H, which, in turn, would retard the transport of H into the Zr metal through the oxide layer, as suggested by Lim *et al.*[35]. These particles would not contribute to the migration of H in the bridging SPPs model.

Finally, the current results suggest that Zr_2Ni-like intermetallic particles may also act as sinks for H atoms when these have reached the Zr metal, provided there is no hindrance in the migration process of H at the interface between the Zr matrix and the SPPs. Consequently, if these particles are dissolved late on in the life of the fuel (as a result of radiation damage or thermal spikes) the trapped H may be released again into the Zr matrix.

In the current study we have considered the enthalpy of solution of H in those binary intermetallics that relate to the most common SPPs found in Zircaloy. These SPPs are reported to be ternary solid solutions[10–12], and in ternary compounds the enthalpy of solution may differ slightly due to electronic and elastic interaction of H with the solutes. This is the subject of further work and beyond the scope of the current letter.

4. Conclusions

The enthalpy of solution of H was calculated for α, β-Zr and the Zr-Cr, Zr-Fe and Zr-Ni intermetallic phases that are relevant to Zry-2 and Zry-4 nuclear fuel cladding.

In Zr (both α and β) the tetrahedral site exhibits a slightly more favourable solution enthalpy for interstitial H compared to the octahedral site. A similar trend is found in each of the intermetallic phases investigated, but in addition, the sites with the largest fraction of neighbouring Zr atoms exhibit the lowest solution enthalpy.

The current study highlights that $ZrCr_2$ and $ZrFe_2$, the boundary phases of the $Zr(Cr,Fe)_2$ solid solution are unfavourable for H accommodation compared

to α-Zr. Conversely, the end members of the Zr_2(Fe,Ni) solid solution accommodate hydrogen readily, even compared to α-Zr. Thus, following Hatano's model of H migration through the cladding oxide layer, we propose that the presence of partially metallic Zr(Cr,Fe)$_2$ SPPs will aid the transport of H through the oxide, while Zr_2(Fe,Ni) SPPs are not helpful, trapping the migrating H until these SPPs are dissolved or oxidised. Therefore, the reason for the decrease in HPUF with decreasing Ni content in Zry-4 must be explained using models other than the one first proposed by Hatano.

5. Acknowledgements

We would like to thank the EPSRC, ANSTO and the UK-MOD for financial support. We also acknowledge Imperial College HPC for the use of resources. M.R. Wenman acknowledges support from EDF Energy through a Fellowship scheme.

[1] G. P. Sabol, in: P. Rudling, B. Kammenzind (Eds.), Zirconium in the Nuclear Industry: 14th International Symposium, volume 1467 of *ASTM-STP*, pp. 3–24.

[2] H. Okamoto, J. Phase Equilib. Diffus. 31 (2010) 411–412.

[3] M. Yao, J. Wang, J. Peng, B. Zhou, Q. Li, in: P. Barberis (Ed.), Zirconium in the Nuclear Industry: 16th International Symposiumy, volume 1529 of *ASTM-STP*, pp. 466–495.

[4] Y. Hatano, K. Isobe, R. Hitaka, M. Sugisaki, J. Nucl. Sci. Technol. 33 (1996) 944–949.

[5] K. Kakiuchi, N. Itagaki, T. Furuya, A. Miyazaki, Y. Ishii, S. Suzuki, T. Terai, M. Yamawaki, in: P. Rudling, B. Kammenzind (Eds.), Zirconium in the Nuclear Industry: 14th International Symposium, volume 1467 of *ASTM-STP*, pp. 349–366.

[6] P. Bossis, D. Pecheur, K. Hanifi, J. Thomazet, M. Blat, in: P. Rudling, B. Kammenzind (Eds.), Zirconium in the Nuclear Industry: 14th International Symposium, volume 1467 of *ASTM-STP*, pp. 494–525.

[7] T. Murai, T. Isobe, Y. Takizawa, Y. Mae, B. Cox, M. Maguire, A. T. Motta, in: G. Saboll, C. Moan (Eds.), Zirconium in the Nuclear Industry: 12th International Symposium, volume 1354 of *ASTM-STP*, pp. 623–640.

[8] G. Lelièvre, C. Tessier, X. Iltis, B. Berthier, F. Lefebvre, J. Alloys Compd. 268 (1998) 308–317.

[9] D. Shaltiel, I. Jacob, D. Davidov, J. Less-Common Met. 53 (1977) 117–131.

[10] P. Chemelle, D. Knorr, J. Van Der Sande, R. Pelloux, J. Nucl. Mater. 113 (1983) 58–64.

[11] W. Yang, R. Tucker, B. Cheng, R. Adamson, J. Nucl. Mater. 138 (1986) 185–195.

[12] N. Bangaru, J. Nucl. Mater. 131 (1985) 280–290.

[13] T. Y. Yang, G. P. Yu, L. J. Chen, J. Nucl. Mater. 150 (1987) 67–77.

[14] E. Vitikainen, P. Nenonen, J. Nucl. Mater. 78 (1978) 362–373.

[15] R. Versaci, M. Ipohorski, J. Nucl. Mater. 80 (1979) 180–183.

[16] V. Krasevec, J. Nucl. Mater. 98 (1981) 235–237.

[17] R. Kuwae, K. Sato, E. Higashinakagawa, J. Kawashima, S. Nakamura, J. Nucl. Mater. 119 (1983) 229–239.

[18] J. Van Der Sande, A. Bement, J. Nucl. Mater. 52 (1974) 115–118.

[19] R. Versaci, M. Ipohorski, J. Nucl. Mater. 116 (1983) 321–323.

[20] G. Lelièvre, D. Fruchart, P. Convertc, F. Lefèvre-Joud, J. Alloys Compd. 347 (2002) 288–294.

[21] H. Okamoto, J. Phase Equilib. Diffus. 28 (2007) 409–409.

[22] S. J. Clark, M. D. Segall, C. J. Pickard, P. J. Hasnip, M. I. J. Probert, K. Refson, M. C. Payne, Zeitschrift für Kristallographie 220 (2005) 567–570.

[23] C. Domain, R. Besson, A. Legris, Acta Mater. 50 (2002) 3513–3526.

[24] J. P. Perdew, K. Burke, M. Ernzerhof, Phys. Rev. Lett. 77 (1996) 3865–3868.

[25] H. J. Monkhorst, J. D. Pack, Phys. Rev. B 13 (1976) 5188–5192.

[26] M. Methfessel, A. Paxton, Phys. Rev. B 40 (1989) 3616–3621.

[27] H. Okamoto, J. Phase Equilib. Diffus. 27 (2006) 548–549.

[28] J. Kearns, J. Nucl. Mater. 22 (1967) 11.

[29] S. C. Lumley, S. T. Murphy, P. A. Burr, R. W. Grimes, P. R. Chard-Tuckey, M. R. Wenman, The Stability of Alloying Agents in Zirconium, 2012. Submitted to J. Nucl. Mater.

[30] D. R. Lide, Handbook of Chemistry and Physics, 90th edition, CRC, 90 edition, 2010.

[31] T. Hahn (Ed.), International Tables for Crystallography, volume A of *International Tables for Crystallography*, International Union of Crystallography, Chester, England, 1993.

[32] S. Yamanaka, K. Higuchi, M. Miyake, Journal of Alloys and Compounds 231 (1995) 503–507.

[33] C. E. Ells, A. D. Mcquillan, J. Inst. Met. 85 (1956) 89–96.

[34] M. W. Mallett, W. M. Albrecht, Journal of The Electrochemical Society 104 (1957) 142.

[35] B. Lim, H. Hong, K. Lee, Journal of nuclear materials 312 (2003) 134–140.

Table 1: Supercells adopted for each of the phases, in terms of the number (p, q, r) of repeats of the basic crystallographic unit cell parameters $\boldsymbol{a}$, $\boldsymbol{b}$ and $\boldsymbol{c}$, the total number of non-hydrogen atoms N, the shortest distance d between defect images in Å, as well as the equivalent hydrogen concentration [H] in *wt* ppm.

Phase	Space Group	p q r	N	d	[H]
α-Zr	$P6_3/mmc$	5 5 3	150	15.6	73.7
β-Zr	$Im\bar{3}m$	4 4 4	128	14.3	86.3
α-$ZrCr_2$ *C15*	$Fd\bar{3}m$	2 2 2	192	14.3	80.7
β-$ZrCr_2$ *C36*	$P6_3/mmc$	2 2 1	96	10.1	161.3
γ-$ZrCr_2$ *C14*	$P6_3/mmc$	2 2 2	96	10.2	161.3
$ZrFe_2$ *C15*	$Fd\bar{3}m$	2 2 2	192	14.1	77.6
$ZrFe_2$ *C36*	$P6_3/mmc$	2 2 1	96	10.0	155.2
$ZrFe_2$ *C14*	$P6_3/mmc$	2 2 2	96	10.0	155.2
Zr_2Fe	$I4/mcm$	2 2 2	96	9.8	132.2
Zr_2Ni	$I4/mcm$	2 2 2	96	10.5	130.6

Table 2: Enthalpy of solution of H in Zr in eV The value by Domain *et al.* is from DFT simulations, the others are all experimentally derived from pressure-concentration-temperature studies.

Ref.	α-Zr	β-Zr
Current	-0.464	-0.619
Domain[23]	-0.600	
Yamanaka[32]	-0.424	-0.455
Ells[33]	-0.473	-0.688
Mallett[34]	-0.373	-0.077
Kearn s[28]	-0.513$\pm$0.09	

Table 3: Enthalpy of solution for an interstitial H in Zr and its intermetallic phases. Positions are expressed following Wyckoff notation. ΔE^H_{sol} is the difference in enthalpy of solution of H in the given intermetallic, compared to the tetrahedral site in α-Zr.

Phase	Position	E^H_{sol} (eV)	ΔE^H_{sol}(eV)
α-Zr	tet-*4f*	-0.46	–
	oct-*2a*	-0.38	0.09
β-Zr	tet-*12d*	-0.62	-0.16
	oct-*6b*	-0.41	0.05
α-$ZrCr_2$ (*C15*)	tet-*96g*	-0.30	0.16
β-$ZrCr_2$ (*C36*)	tet-*6h*	-0.28	0.19
γ-$ZrCr_2$ (*C14*)	tet-*6h*	-0.36	0.10
$ZrFe_2$ (*C15*)	tet-*96g*	0.04	0.50
$ZrFe_2$ (*C36*)	tet-*6h*	0.04	0.50
$ZrFe_2$ (*C14*)	tet-*6h*	0.03	0.50
Zr_2Fe	tet-*16l*	-0.45	0.01
Zr_2Ni	tet-*16l*	-0.67	-0.20

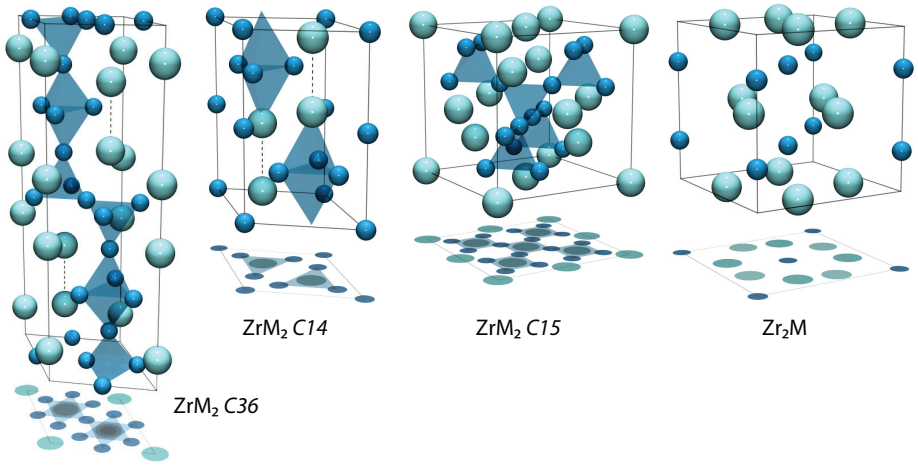

Figure 1: Unit cells of *C36*, *C14*, *C15* Laves structure and of Zr_2M. The larger lighter spheres represent the Zr atoms, the smaller darker spheres represent Cr or Fe in the laves phases and Fe or Ni in the Zr-rich phase.